ELSEVIER

Contents lists available at ScienceDirect

Applied Computing and Geosciences

journal homepage: www.sciencedirect.com/journal/applied-computing-and-geosciences





Electrical anisotropy calculation of the continental crust by resistor network-based circuit simulations

Song Luo^{a,b}, Haiying Hu^{a,*}, Lidong Dai^{a,**}

- a Key Laboratory of High-Temperature and High-Pressure Study of the Earth's Interior, Institute of Geochemistry, Chinese Academy of Sciences, Guiyang, 550081, China
- b University of Chinese Academy of Sciences, Beijing, 100039, China

ARTICLE INFO

Dataset link: Random-Resistor-Network (Original data)

Keywords:
Magnetotellurics
Electrical anisotropy
Random resistor network
Microfabrics
Continental crust

ABSTRACT

Electrical anisotropy has been broadly observed by magnetotelluric (MT) surveys in the continental crust. It is proposed to be caused by rock microfabrics, lithologic layering, or oriented alignment of fluid or melt in rocks, whereas the validity of these mechanisms has not yet been verified due to the lack of experimental and computational evidence. Laboratory measurements on the electrical anisotropy of crustal rocks are extremely challenging when considering microfabrics and oriented microcracks filled with fluid. In contrast, numerical modeling, being an efficient approach, can be used to compute the anisotropic physical properties of rocks. In this study, the electrical anisotropy of crustal rocks was first modeled by circuit simulation techniques using a random resistor network model, based on the lattice-preferred orientation, modal compositions, and mineral electrical conductivity. The results indicate that the conversion from single crystals to the corresponding aggregates leads to a great reduction in electrical anisotropy, particularly for quartz single crystal with high anisotropy. Moreover, the electrical anisotropy of two-phase aggregates decreases with the increasing proportion of the second low-anisotropy minerals (e.g., plagioclase), such as from quartzite to granite. For layered lithology, the lower-crustal gabbro has higher electrical anisotropy compared to middle-crustal quartz-bearing rocks. The modeled electrical anisotropy from the middle to lower crust matches well with the geophysical observations in the Central Great Basin.

1. Introduction

Electrical anisotropy in the crust and upper mantle has been revealed to be broadly present by magnetotelluric (MT) sounding (Brasse et al., 2009; Le Pape et al., 2012; Kapinos et al., 2016; Liu et al., 2019, 2021). It can be identified through various signatures, such as inconsistency in transverse electric and transverse magnetic responses (Heinson and White, 2005; Le Pape et al., 2012), deflection of induction vectors (Brasse and Eydam, 2008; Brasse et al., 2009), and phases rolling out of quadrant (Heise and Pous, 2003). Several main mechanisms have been proposed as the origin of these electrical anisotropy anomalies including anisotropic distribution of conductive phases (Wannamaker, 2005), lithologic layering (Yang, 2011), and oriented alignment of fluid or melt in rocks (Le Pape et al., 2012; Zhang et al., 2014; Pommier et al., 2015). All of these mechanisms are closely associated with rock microfabrics, e. g., lattice-preferred orientations (LPOs), grain shape, grain boundary distribution (Simpson, 2013; Almqvist and Mainprice, 2017). However,

experimental evidence for these mechanisms is insufficient since present studies mainly concentrate on the anisotropic electrical conductivity of mineral single crystals rather than rocks. Moreover, direct measurement on the electrical anisotropy of crustal rocks is challenging when considering various factors that affect rock anisotropy (e.g., LPOs and oriented fluid). Numerical simulation of mantle rocks has demonstrated that the electrical anisotropy of polycrystal aggregates is orders of magnitude lower than that of single crystals (Simpson and Tommasi, 2005). This implies that the use of single crystals is inappropriate for interpreting the significant electrical anisotropy observed in complex rock systems. Numerical modeling is used extensively to calculate other anisotropic physical properties of rocks such as seismic velocity and thermal diffusivity (Hacker et al., 2014; Gibert and Mainprice, 2009; Almqvist and Mainprice, 2017). Thus, numerical modeling would be an effective tool to calculate the electrical anisotropy of the crust based on rock microfabric and electrical conductivity data of the constituent minerals.

E-mail addresses: huhaiying@vip.gyig.ac.cn (H. Hu), dailidong@vip.gyig.ac.cn (L. Dai).

^{*} Corresponding author.

^{**} Corresponding author.

Currently, isotropic electrical conductivity of rocks has been extensively simulated by multiphase conduction models, such as Hashin-Shtrikman bounds (Hashin and Shtrikman, 1962; Hu et al., 2022), series and parallel models (Schulgasser, 1976; Xu et al., 2000), and geometric mean model (Shankland and Duba, 1990). Whereas anisotropic electrical conductivity models are relatively uncommon. A network model was first introduced by Kirkpatrick (1973) to calculate the anisotropic conductivity of heterogeneous conductors. This model was further optimized to establish the link between the crustal fracture network and electrical field distortion (Bahr, 1997, 2000). Subsequently, this model was used to the electrical anisotropy calculations of mantle peridotite based on anisotropic hydrogen diffusion and LPOs of hydrated olivine (Simpson, 2002, 2013; Simpson and Tommasi, 2005). More recently, Kirkby et al. (2016) employed random resistor network models to explore the relationship between electrical resistivity and permeability in fractured rocks. A series-parallel model was also applied to the electrical anisotropy calculations of the upper mantle (Pommier et al., 2015); however, this model did not take into account the intrinsic electrical anisotropy associated with mineral texture (e.g., LPOs). It is well known that the properties of mineral single crystal significantly determine the macroscopic properties of rocks (Bahr, 2000; Gatzemeier and Tommasi, 2006; Fuji-ta et al., 2018). Although there are numerous data on the anisotropic electrical anisotropy and texture of the crustal minerals (Yang, 2012; Czertowicz et al., 2019; Hu et al., 2024), the electrical anisotropy of the crustal rocks has yet to be systematically modeled.

Resistor network models are a numerical simulation technique that effectively discloses electrical conduction by modeling an interconnected grid of resistors as a heterogeneous medium. As usual, it can be widely applied to model complex transport processes, such as electrical conduction of heterogeneous rocks (Kirkpatrick, 1973; Bahr, 2000; Simpson and Tommasi, 2005; Kirkby et al., 2016). It is well known that this model has many available advantages such as flexibility, scalability, and the ability to incorporate microscopic characterizations (e.g., physical properties of mineral single crystal, crystallographic orientation, and modal composition). In comparison with other numerical simulation techniques, the resistor network models can well represent the physical behavior of the natural rocks, especially regarding LPOs and lithological heterogeneity. Therefore, it is more appropriate for exploring the electrical anisotropy of complex crustal rock systems, which is mainly caused by the intrinsic mineral anisotropy and rock microstructure.

In this study, we first adopted circuit simulation techniques to compute crustal electrical anisotropy using resistor network models that were based on the modal mineral composition, LPOs, and conductivity of crustal rock-forming minerals. The electrical anisotropy of single-phase, two-phase, and lithologic layering aggregates were separately calculated. The results were in agreement with the electrical anisotropy anomalies from MT responses in the Central Great Basin (CGB). More importantly, the resistor network models proposed in this study are able to systematically simulate complex sources of electrical anisotropy and reproduce geophysical observations.

2. Computational framework

This study develops a numerical simulation method to quantify the macroscopic electrical anisotropy of complex crustal rock systems. Specifically, we used the resistor network models that incorporate the physical properties of mineral single crystal, LPOs, and modal mineral compositions to simulate the electrical conduction in the rock systems. This section outlines the computational procedures adopted to construct the resistor network models and describes the geological parameterization of the specific rocks.

2.1. Electrical anisotropy from single crystal to aggregates

The electrical properties of rocks are dominated by the constituent minerals. In general, the continental crust is predominantly composed of silicate minerals including quartz, feldspar, and pyroxene (Rudnick and Gao, 2003). The LPOs of these rock-forming minerals govern the intrinsic electrical anisotropy of the crust through crystallographic alignment (Gatzemeier and Tommasi, 2006; Mainprice et al., 2011). The macroscopic electrical anisotropy of the crust can be obtained by modeling current flow in the primary rock-forming minerals according to their crystallographic orientation and conductivity data. This conduction model can be constructed using a random resistor network. The details for the calculation of electrical anisotropy are outlined in the following steps.

- (1) Gather mineral LPO and conductivity data. To obtain the intrinsic electrical anisotropy of crustal rocks, the LPOs of the major minerals, i.e., quartz and plagioclase, were taken from previously published electron back-scattered diffraction (EBSD) measurements on naturally deformed rocks (Czertowicz et al., 2019; Allard et al., 2021). Clinopyroxene LPOs were excluded because the conductivity of clinopyroxene is almost isotropic (Yang, 2012), thus contributing little to the bulk electrical anisotropy of rocks. Grains with small sizes (1 pixel) were selected for crystallographic orientation analysis, and orientation data were tabulated as Euler angles ($\varphi_1, \Phi, \varphi_2$). Electrical conductivity data of primary minerals in the middle and lower crust are summarized in Table 1.
- (2) **Build orientation matrix.** Although slip systems change with temperature, our model only considered the typical slip system of crustal minerals. Taking quartz with prism<a> slip system as a representative (Passchier and Trouw, 2005), a crystal near the maximum density direction (Fig. 1a) was identified in the corresponding pole figure (Fig. 1c). Crystallographic directions of *a*, *b*, and *c* can be formulated by an orientation matrix **g**:

$$\mathbf{g} = \begin{bmatrix} u & r & h \\ v & s & k \\ w & t & l \end{bmatrix} \tag{1}$$

where $[u\ v\ w]$, $[r\ s\ t]$ and $[h\ k\ l]$ represent three mutually perpendicular directions of crystals. The matrix comprises components of the crystal unit vectors in the reference coordinate frame.

(3) **Define electrical anisotropy in the reference frame.** In the matrix **g**, the *u*, *r*, *h* and *w*, *t*, *l* correspond to the components of three crystallographic directions along the reference coordinate axes *X* and *Y*, respectively. Therefore, the electrical anisotropy of quartz in the *X-Y* reference system is derived as:

$$\frac{\sigma_{Y}}{\sigma_{X}} = \frac{w \times \sigma_{u \vee w} + t \times \sigma_{r s t} + l \times \sigma_{h k l}}{u \times \sigma_{u \vee w} + r \times \sigma_{r s t} + h \times \sigma_{h k l}}$$
(2)

where σ_X and σ_Y are conductivities of crystal along the X and Y directions. σ_{uvw} , σ_{rst} , and σ_{hkl} are electrical conductivity tensors for

Table 1
Details of conductivity and orientation data used for electrical anisotropy simulations.

Crustal minerals	Conductivity data	EBSD	H ₂ O content (ppm)
Quartz	Hu et al. (2024)	Czertowicz et al. (2019)	42
Plagioclase	Yang (2011)	Allard et al. (2021)	135
Clinopyroxene	Yang et al. (2011)		270

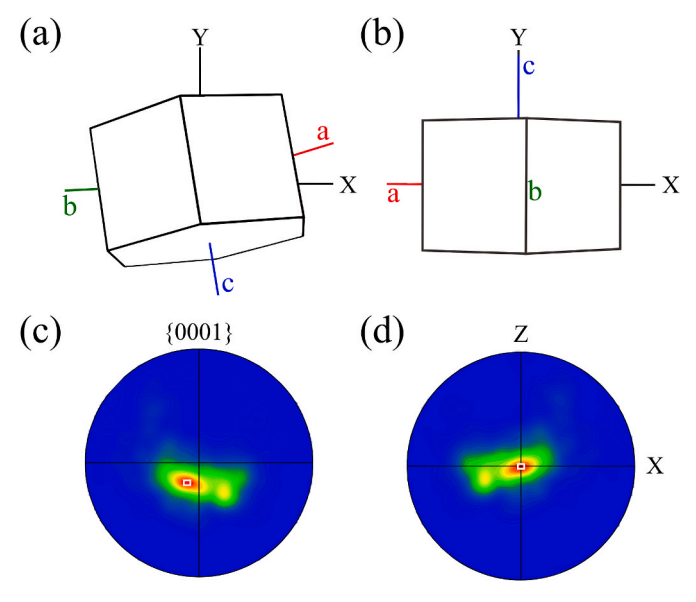


Fig. 1. Crystal orientation of quartz single crystals and associated EBSD pole figures. (a) and (b) Crystallographic orientations of the quartz crystal acquired before and after coordinate rotation, respectively. (c) and (d) Corresponding pole figures illustrated using lower hemisphere equal-area projections before and after coordinate rotation, respectively.

respective crystallographic directions of quartz single crystal.

- (4) **Rotate reference coordinate system.** Since the quartz single crystal has maximum conductivity along the *c*-axis, the maximum-density point direction for the *c*-axis observed by the pole figure (Fig. 1c) matches the maximum-conductivity direction of aggregates. To quantify the maximum conductivity of the aggregates, the reference coordinate system was rotated to align the *Y*-axis with the maximum density direction of the *c*-axis (Fig. 1b and d).
- (5) Convert to Euler angles and apply statistical analysis. In step 5, the orientation matrix **g** was converted to Euler angles (φ_1, Φ , φ_2) (Bunge, 1982):

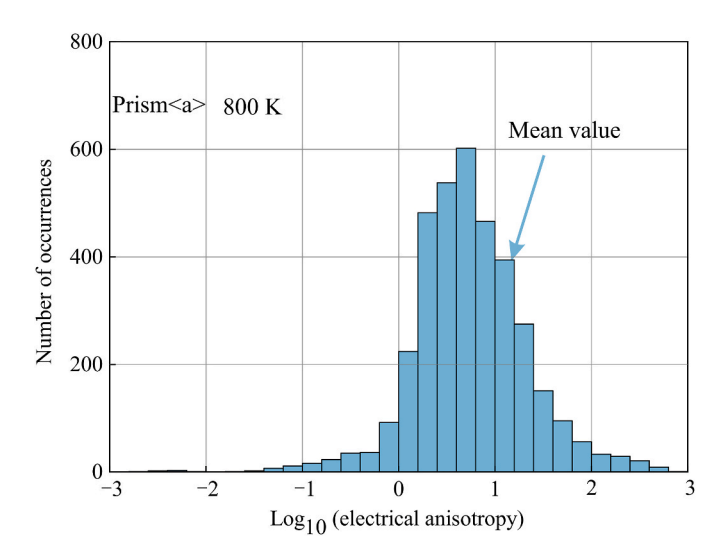


Fig. 2. Electrical anisotropy distribution function of single crystals with quartz prism<a> slip system at 800 K.

microscopic scale (single crystal) and macroscopic scale (rocks). As illustrated in Fig. 3a and b, individual crystals were modeled as resistor pairs that make up the resistor network, where the resistance values of the resistor pair in the X and Y directions correspond to quartz resistivities along these two directions. In the random resistor network, $n \times n$ Y-direction resistors and $(n-1) \times (n-1)$ X-direction resistors were arranged (Fig. 3c). The electrical anisotropy distribution function obtained from Step 5 determines the probability distribution of resistor pairs within the network, with resistance values scaled down proportionally to optimize the subsequent simulations. The boundaries (in red) of the resistor network were short-circuited as electrodes to emulate laboratory measurement conditions. To apply voltage across the resistor network in the X and Y directions, we adjusted the boundaries to generate a new network (Fig. 3d). Subsequently, a Pathon algorithm was implemented to randomize the resistor pairs within the networks. The random resistor network was separately operated across these two directions through an online electronic circuit simulator (https://lushprojects.com/circ uitjs/) to obtain the respective currents. Bulk electrical anisot-

$$\begin{bmatrix} u & r & h \\ v & s & k \\ w & t & l \end{bmatrix} = \begin{bmatrix} \cos \varphi_1 \cos \varphi_2 - \sin \varphi_1 \sin \varphi_2 \cos \Phi & \sin \varphi_1 \cos \varphi_2 + \cos \varphi_1 \sin \varphi_2 \cos \Phi & \sin \varphi_2 \sin \Phi \\ -\cos \varphi_1 \sin \varphi_2 - \sin \varphi_1 \cos \varphi_2 \cos \Phi & -\sin \varphi_1 \sin \varphi_2 + \cos \varphi_1 \cos \varphi_2 \cos \Phi & \cos \varphi_2 \sin \Phi \\ \sin \varphi_1 \sin \Phi & -\cos \varphi_1 \sin \Phi & \cos \Phi \end{bmatrix}$$
(3)

Subsequently, the electrical anisotropy of a single crystal in the X-Y reference coordinate system can be obtained by substituting Eq. (3) into Eq. (2). To validate the simulated electrical anisotropy, a reverse calculation was performed using the given angle between the crystal c-axis and the reference Y-axis. Additionally, the electrical anisotropy distribution function of single crystals, which describes the probability that a particular single-crystal anisotropy contributes to the aggregates, was determined by the statistical analysis of all quartz crystals (Fig. 2).

(6) Build a resistor network model. Resistor network models allow us to bridge the gap in electrical anisotropy between the ropy of aggregates was then acquired from the current ratio between Y and X directions ($\sigma_Y/\sigma_X=I_Y/I_X$), which were averaged over multiple calculations of the random resistor network.

Simulation errors mainly include the (i) resistance scaling approximation, (ii) randomization-induced uncertainty in resistor pair distributions, (iii) boundary condition artifacts during network adjustments, and (iv) calculated fluctuations arising from the size of resistor networks (n). To minimize these errors, 100 random resistor networks were separately simulated for various network sizes (ranging from 10 to 40), and the results display that the convergence of calculated anisotropy has a positive correlation with the network size (Fig. 4). The variation in average electrical anisotropy for networks with n values from 10 to 40 is

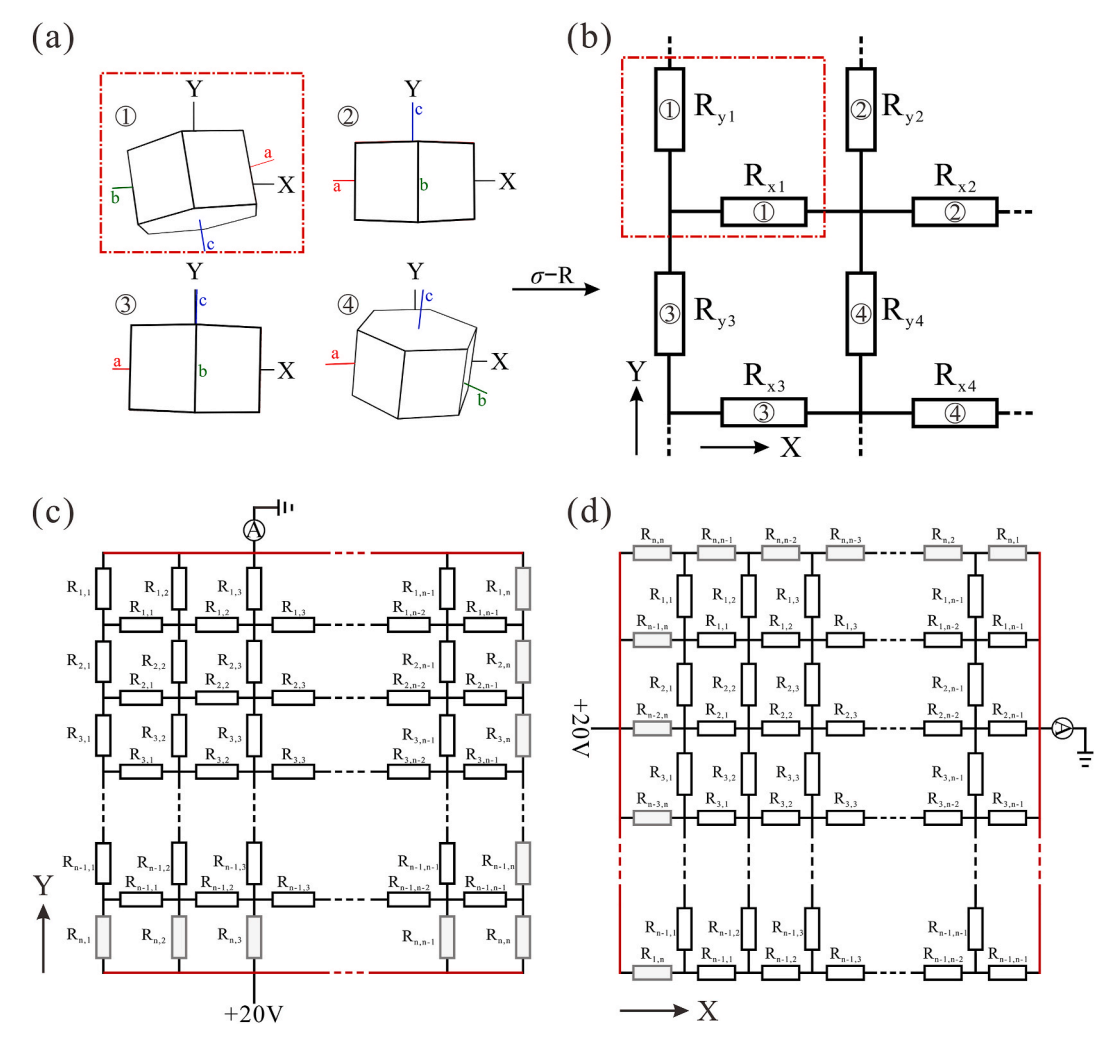


Fig. 3. Conversion of electrical anisotropy from single crystal to polycrystalline aggregates based on electronic circuit simulation. (a) A single crystal is modeled as a resistor pair. (b) Resistor pairs within a resistor network. Random resistor networks with voltage applied equivalently in the *Y*-direction (c) and *X*-direction (d), where the *Y*-boundary resistances are converted to the corresponding *X*-boundary resistances.

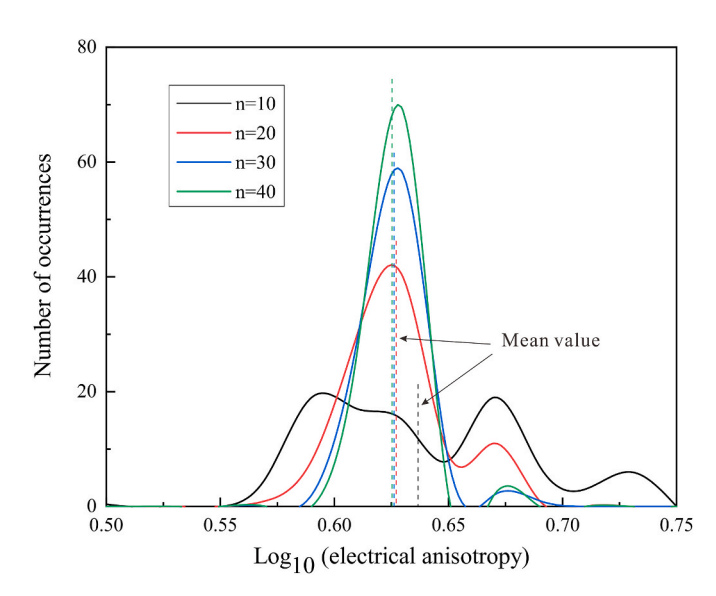


Fig. 4. Electrical anisotropy generated from 100 individual resistor networks with sizes (*n*) ranging from 10×10 to 40×40 .

below 8 %, thus a standardized network size of n=20 (i.e., 400 resistor pairs) is adopted for the subsequent calculations. In this resistor network model, the uncertainties from the network size effects, randomizations, and boundary artifacts are not more than 8 %. In a comprehensive consideration of the resistance scaling approximation, the overall error is estimated to be less than 10 %.

To better visualize the current flow in the network, the simplified 5 \times 5 resistor networks are shown in the videos *RRN-Y* and *RRN-X* available in Supplementary Material.

2.2. Geological model parameterization

The method for single-mineral aggregates can be extended to simulate more complex rocks composed of various minerals equilibrated under crustal thermodynamic conditions. Accordingly, we established two-phase models of the middle and lower crust. The former consists of randomly distributed quartz and plagioclase, and the latter comprises plagioclase and clinopyroxene. In these models, the electrical anisotropy of plagioclase single crystal is neglected in the middle crust as quartz has much higher anisotropy than plagioclase (Fig. 5a) (Wang et al., 2010; Yang, 2012; Hu et al., 2024), but it is considered in the lower crust due to the weaker electrical anisotropy of clinopyroxene. In addition, mineralogical proportions significantly influence not only the isotropic electrical conductivity of rocks (Pommier and Le-Trong, 2011; Dai et al., 2014; Sun et al., 2019; Wang et al., 2022), but also the anisotropic

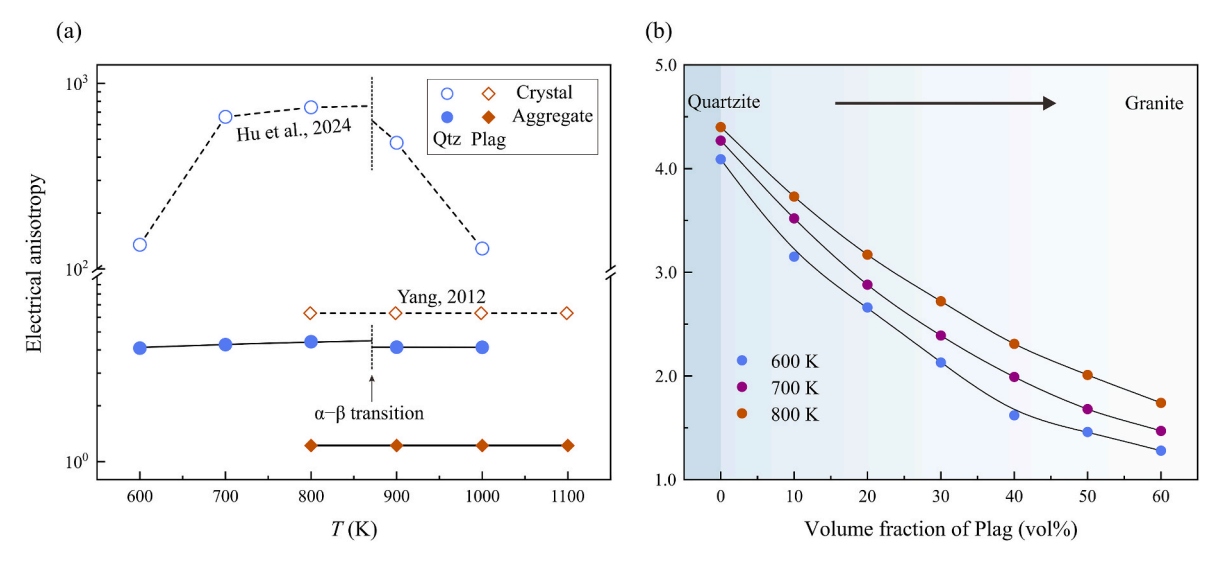


Fig. 5. Electrical anisotropy of single- and two-phase aggregate models. (a) Electrical anisotropy of single-phase aggregates (Qtz and Plag) as a function of temperature. The hollow circle (green) and diamond (orange) represent the anisotropic conductivity of quartz (Hu et al., 2024) and plagioclase (Yang, 2012) single crystals, respectively. (b) Electrical anisotropy of two-phase aggregates (Qtz + Plag) as a function of mineralogical proportion. Abbreviations: Qtz. quartz, Plag: plagioclase. (For interpretation of the references to colour in this figure legend, the reader is referred to the Web version of this article.)

Table 2 Partial parameters for electrical anisotropy simulations. T is temperature, P is pressure, and M is modal mineral composition.

	Models	Phase	T (K)	P (GPa)	M
Middle crust	Single- phase	Qtz	600–1000	1.0	Qtz ₁₀₀
	Two- phase	Qtz + Plag	600–800	1.0	$Qtz_{100\sim40}Plag_{0\sim60}$
	Layered	Qtz/Qtz + Plag	600–800	1.0	Qtz _{90~40} Plag _{10~60}
Lower crust	Single- phase	Plag	800–1100	1.0	Plag ₁₀₀
	Layered	Plag-rich/ Cpx-rich	800–1000	1.0	Plag _{66~54} Cpx _{34~46}

Abbreviations: Qtz: Quartz, Plag: Plagioclase, Cpx: Clinopyroxene.

conductivity. As a result, the mineralogical proportions in the context of the middle and lower crust are given in Table 2 for the anisotropy simulations. Furthermore, there is increasing evidence that lithologic layering is the origin of the crustal electrical anisotropy (Wannamaker, 2005; Yang et al., 2011). Therefore, we established layered models for the middle crust (interbedded quartz layers and quartz-plagioclase layers) and lower crust (plagioclase-rich layers and clinopyroxene-rich layers) based on petrological observations (Dai et al., 2008; Yang et al., 2008; Hou et al., 2023). A layered algorithm was employed to simulate electrical conductivity differences between lithologic layers.

3. The electrical anisotropy of the crust

To quantify the electrical anisotropy of crustal rocks, we conducted numerical simulations on the single-phase, two-phase, and lithologic layered models using the resistor network. These models explore the influence of temperatures, LPOs, mineral proportions, and lithologic layering on the bulk electrical anisotropy of the crustal rocks.

3.1. Single-phase and two-phase aggregate models

Some of mineral single crystals with high electrical anisotropy can account for the anisotropic anomalies in the crust and upper mantle (Wang et al., 2010; Yang, 2012; Dai and Karato, 2014); however, the

conversion from single crystal to aggregates can lead to a dramatical decrease in electrical anisotropy (Simpson and Tommasi, 2005). The electrical anisotropy calculations for quartz and plagioclase aggregates show this feature at 600–1100 K and 1.0 GPa, as illustrated in Fig. 5a. For instance, it decreases almost two orders of magnitude for quartz and from 6.3 to approximately 1.2 for plagioclase. Quartz aggregates exhibit higher anisotropy (i.e., $\sim\!4.0$) compared to plagioclase aggregates (i.e., $\sim\!1.2$), as there is a large difference in electrical anisotropy between quartz and plagioclase single crystals. A discontinuous variation in anisotropy is observed in quartz aggregates due to the occurrence of the quartz $\alpha\!-\!\beta$ transition. This is a phase change from trigonal (α) to hexagonal (β) symmetry, which alters the lattice and affects the electrical conductivity.

A systematic reduction in electrical anisotropy is shown in Fig. 5b for quartz–plagioclase systems as plagioclase content increases (10 %–60%), transitioning from quartzite of around 4.0 to granite of around 1.5. These variations are broadly consistent with olivine–enstatite systems (Simpson and Tommasi, 2005). Electrical anisotropy exhibits a distinct temperature dependence and increases with temperature under middle crustal conditions (Fig. 5b), which is likely attributed to the positive temperature effect on anisotropy in quartz aggregates prior to the α – β transition (Fig. 5a). For the lower-crustal model, plagioclase–clinopyroxene systems generate negligible electrical anisotropy (<1.2), as the weak anisotropy of plagioclase aggregates (~1.2, Fig. 5a) is further weakened by the addition of clinopyroxene.

3.2. Lithologic layered model

Lithologic layering is a pervasive feature in the continental lower crust (Montanini and Harlov, 2006; Dai et al., 2008). The schematics of the resistor networks that represent layered lithologies of the middle and lower crust are illustrated in Fig. 6a and c, respectively. Temperature and mineralogical proportions, as key parameters affecting electrical anisotropy, are systematically considered in these models. The effect of temperature on electrical anisotropy is opposite for the middle and lower crust (Fig. 6b and d), primarily because quartz-dominated anisotropy in the middle crust increases with temperature, while the conductivity difference between the plagioclase-rich (m% Cpx) and clinopyroxene-rich (m% Plag) layers in the lower crust decreases with temperature. The minimum value obtained at 600 K in the middle-crustal model arises from a transition in the dominant

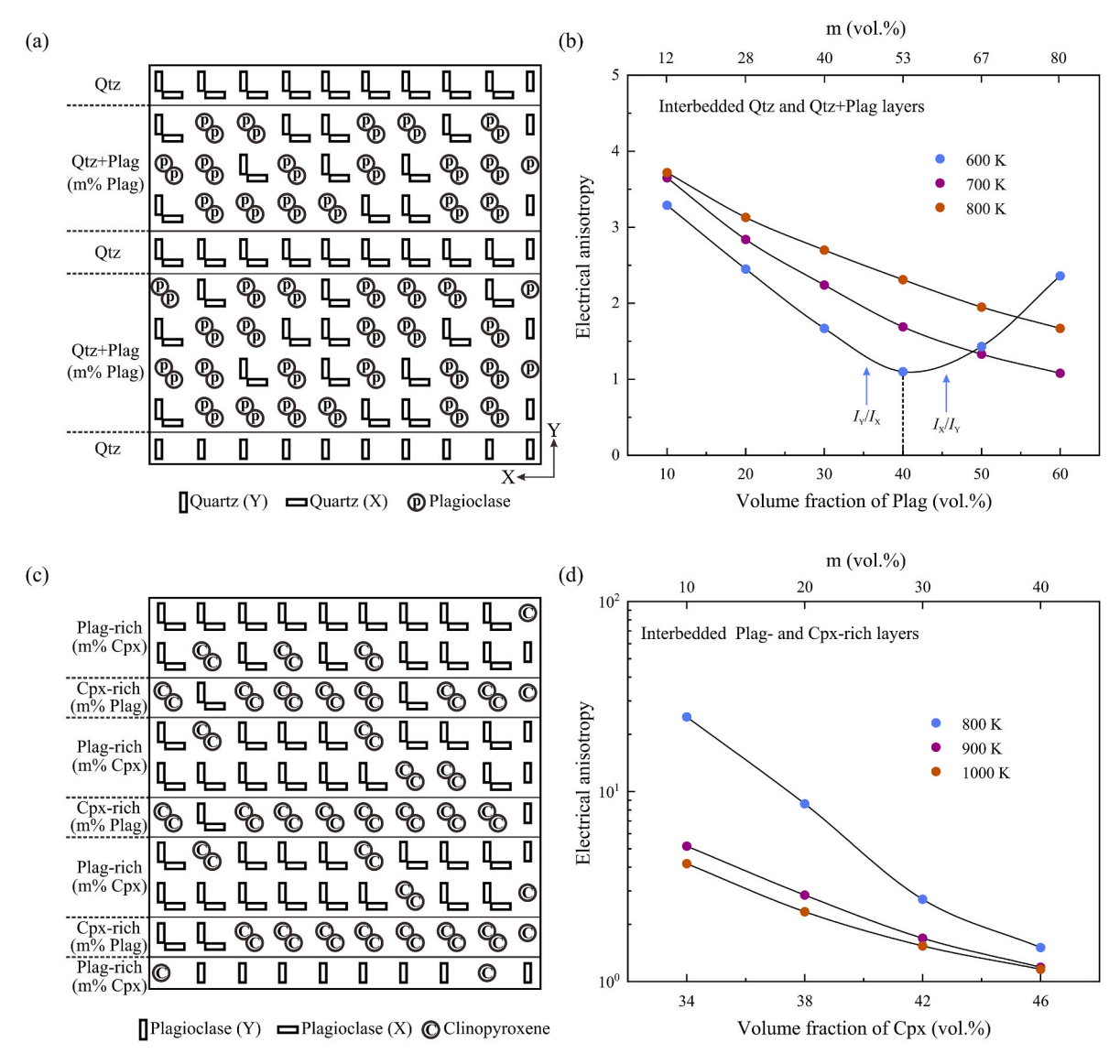


Fig. 6. Schematic diagram of layered resistor network models with a size of 10×10 and corresponding electrical anisotropy. (a) The resistor network consists of Qtz layers and polymineralic (Qtz + Plag) layers for the middle crust, where m% represents the volume fraction of plagioclase in the polymineralic layers. (b) The calculated electrical anisotropy for the middle crust. (c) The network comprises alternating Cpx- and Plag-rich layers for the lower crust, where m% denotes the volume fraction of Cpx in the Plag-rich layers or Plag in the Cpx-rich layers. (d) The calculated electrical anisotropy for the lower crust. Abbreviation: Cpx: Clinopyroxene.

contributor to electrical anisotropy, from quartz LPOs (I_Y/I_X) to lithologic layering (I_X/I_Y) as quartz content decreases. In middle- and lower-crustal models, electrical anisotropy decreases with the addition of plagioclase and clinopyroxene, respectively, as these two minerals weaken the contrasts in conductivity between different layers. Moreover, the lower crust exhibits higher electrical anisotropy (<24.0) than the middle crust (<4.0) (Fig. 6b and d).

4. Comparison of numerical models to magnetotelluric observations

A number of MT surveys have revealed electrical anisotropy in the continental crust, yet its origins are not well understood (Leibecker et al., 2002; Sodergren, 2002; Heinson and White, 2005; Le Pape et al., 2012). Crustal electrical anisotropy of the Central Great Basin was modeled by Sodergren (2002) via 1D inversion of observed MT soundings (Fig. 7a), with a maximum anisotropy ratio of $\sigma_{\rm max}/\sigma_{\rm min} < 8.0$. In this region, the highly conductive graphite was unlikely present due to the high oxygen fugacity associated with volcanic activity (Wannamaker

et al., 1997; Wannamaker, 2005). Oriented alignment of fluid or melt controlled by rock microfabrics was initially suggested as the primary origin of the crustal anisotropy (Wannamaker et al., 1997). However, it can produce relatively high electrical anisotropy based on a previous study (Pommier et al., 2015), which greatly exceeds the observed results in the CGB. LPO and lithologic layering, generating moderate anisotropy according to our simulation results, were thus proposed as potential explanations for the electrical anisotropy observed in the CGB (Wannamaker, 2005; Yang, 2011; Martí, 2013).

To verify the validity of these mechanisms in the CGB, a rock model consisting of felsic middle crust and gabbroic lower crust was constructed with consideration of both the LPOs and lithologic layering, as illustrated in Fig. 7b. The electrical anisotropy of the model was calculated by our circuit simulations under the corresponding thermodynamic conditions (i.e., the heat flow of $q=75~\text{mW/m}^2$) in the CGB (Wannamaker et al., 1997, 2008). For the rock model of the middle crust, although the two-phase aggregate and lithologic layering models produce roughly comparable results under identical mineralogical proportions (Figs. 5b and 6b), the two-phase aggregate model is more

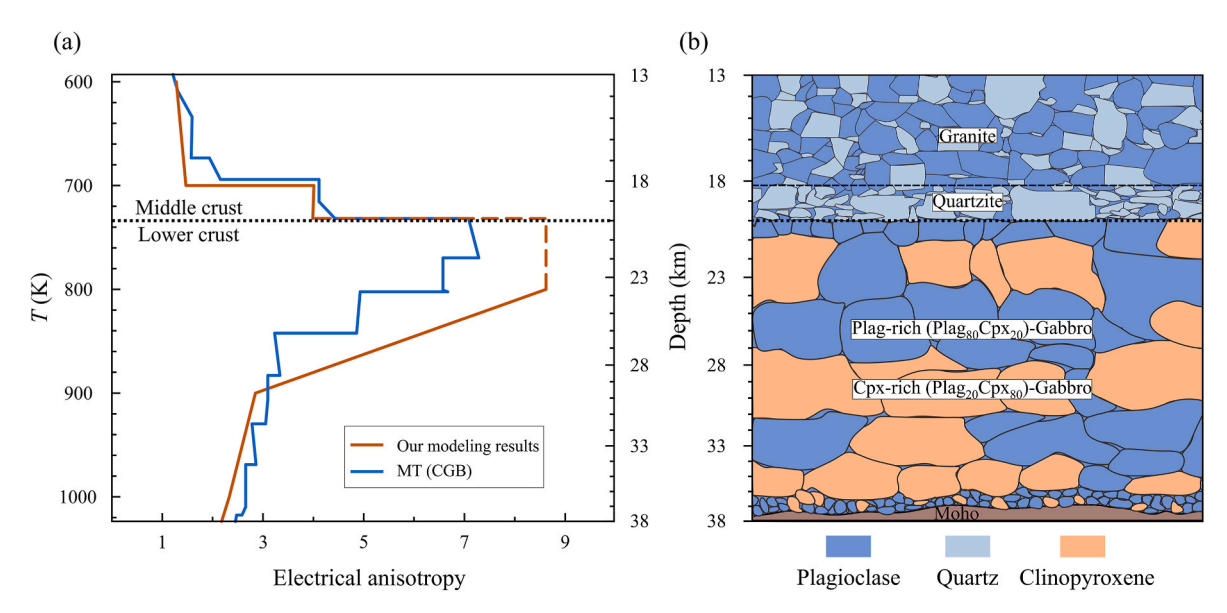


Fig. 7. Sketch of crustal rock model and corresponding simulated electrical anisotropy, applied to the Central Great Basin (Sodergren, 2002). (a) Comparison between modeled and observed crustal electrical anisotropy in the Central Great Basin. The orange and blue lines represent simulated and observed electrical anisotropy, respectively. The grey dotted line corresponds to the boundary of the middle and lower crust. (b) Conceptual 2D model of the crustal structure used in the simulations. This model exhibits the LPO-related fabric and lithologic layering that contribute to electrical anisotropy. (For interpretation of the references to colour in this figure legend, the reader is referred to the Web version of this article.)

suitable to account for the anisotropy anomalies as layered lithology commonly occurs in some local regions (Hou et al., 2023). Our results showed that granite with 40 % quartz and 60 % plagioclase can be responsible for the electrical anisotropy at depths less than 18 km (Fig. 7b). Nevertheless, it cannot account for the anisotropic anomaly of around 4.0 beyond this depth. By contrast, quartzite, comprising 95 % quartz and 5 % plagioclase, exhibits higher electrical anisotropy than granite, providing a plausible explanation for the anisotropic anomaly at the lowermost middle-crust (Fig. 7b). For the lower crust, xenolith observations have indicated that a fabric of interbedded plagioclase-rich and pyroxene-rich layers widely exists at millimeter to centimeter scales (Downes et al., 2002; Montanini and Harlov, 2006; Ulianov and Kalt, 2006; Dai et al., 2008). The modal mineral composition of gabbro composed of alternating 80 % plagioclase +20 % clinopyroxene and 20 % plagioclase +80 % clinopyroxene was adopted in the present model (Fig. 7b), based on the petrological and geophysical studies (Dai et al., 2008; Yang, 2011; Yang et al., 2011). The results showed the layered gabbro could well explain the electrical anisotropy observed in the MT data at depths greater than 20 km (Fig. 7).

In summary, our modeling results derived from electronic circuit simulations are in agreement with geophysical observations in the CGB. Crustal anisotropy anomalies are higher in some other regions (Heinson and White, 2005; Le Pape et al., 2012; Liu et al., 2019), which could be caused by other mechanisms including (1) strong shape-preferred orientation (Gatzemeier and Tommasi, 2006), (2) interconnected network of graphite/sulfide along microfractures (Wannamaker, 2005), and (3) oriented alignment of fluid or melt within rocks (Le Pape et al., 2012; Zhang et al., 2014; Pommier et al., 2015; Taylor-West and Katz, 2015). More complex calculations are required to quantify the electrical anisotropy caused by these mechanisms.

5. Conclusions

Our study first implements circuit simulation techniques to calculate the electrical anisotropy of the crust based on random resistor network that incorporates the mineral conductivity data and rock microfabrics. The results indicate that there is a significant reduction in electrical anisotropy from single crystals to aggregates, and a further reduction is observed with the addition of the low-anisotropy mineral phases. In

addition, lithologic layering in gabbroic lower-crustal rocks have notably higher anisotropy than quartz-rich rocks in the middle crust. Our results show that the electrical anisotropy simulated using our random resistor network model is in agreement with magnetotelluric observations over the Central Great Basin.

5.1. Computer Code Availability

Name of the library: Random-Resistor-Network.

Contact: luosong@mail.gyig.ac.cn.

Program language: Python 3.9.7.

Program size: 50 KB.

The source codes in this work are available at https://github.com/Songluo428/Random-Resistor-Network.

CRediT authorship contribution statement

Song Luo: Writing – original draft, Visualization, Validation, Software, Methodology, Investigation, Formal analysis, Data curation, Conceptualization. **Haiying Hu:** Writing – review & editing, Supervision, Project administration, Methodology, Investigation, Funding acquisition, Formal analysis, Conceptualization. **Lidong Dai:** Writing – review & editing, Supervision, Project administration, Methodology, Investigation, Funding acquisition, Formal analysis, Conceptualization.

Declaration of competing interest

The authors declare that they have no known competing financial interests or personal relationships that could have appeared to influence the work reported in this paper.

Acknowledgments

We thank Anna Martí and an anonymous reviewer for their very helpful comments and suggestions in the reviewing process, which helped us greatly in improving the manuscript. This study was financially supported by the National Natural Science Foundation of China (Grant Nos. 42274137).

Appendix A. Supplementary data

Supplementary data to this article can be found online at https://doi.org/10.1016/j.acags.2025.100265.

Data availability

I have shared the link to my data/code at the attach file step. Random-Resistor-Network (Original data) (GitHub)

References

- Allard, M., Ildefonse, B., Oliot, É., Barou, F., 2021. Filtered EBSD dataset in slow spread Oceanic gabbros. IODP Expedition 360. PANGAEA. https://doi.org/10.1594/PA
- Almqvist, B.S.G., Mainprice, D., 2017. Seismic properties and anisotropy of the Continental crust: predictions based on mineral texture and rock microstructure. Rev. Geophys. 55 (2), 367–433. https://doi.org/10.1002/2016RG000552.
- Bahr, K., 1997. Electrical anisotropy and conductivity distribution functions of fractal random networks and of the crust: the scale effect of connectivity. Geophys. J. Int. 130, 649–660. https://doi.org/10.1111/j.1365-246X.1997.tb01859.x.
- Bahr, K., 2000. Percolation in the crust derived from distortion of electric fields. Geophys. Res. Lett. 27 (7), 1049–1052. https://doi.org/10.1029/1999GL005430.
- Brasse, H., Eydam, D., 2008. Electrical conductivity beneath the Bolivian orocline and its relation to subduction processes at the south American Continental margin. J. Geophys. Res. 113 (B7), B07109. https://doi.org/10.1029/2007JB005142.
- Brasse, H., Kapinos, G., Li, Y., Mütschard, L., Soyer, W., Eydam, D., 2009. Structural electrical anisotropy in the crust at the south-central Chilean Continental margin as inferred from geomagnetic transfer functions. Phys. Earth Planet. Inter. 173 (1), 7–16. https://doi.org/10.1016/j.pepi.2008.10.017.
- Bunge, H.-J., 1982. Texture Analysis in Materials Science. Butterworths, London, p. 595. https://doi.org/10.1016/C2013-0-11769-2.
- Czertowicz, T.A., Takeshita, T., Arai, S., Yamamoto, T., Ando, J.-I., Shigematsu, N., Fujimoto, K.-I., 2019. The architecture of long-lived fault zones: insights from microstructure and quartz lattice-preferred orientations in mylonites of the median tectonic line, SW Japan. Prog. Earth Planet. Sci. 6 (1), 25. https://doi.org/10.1186/s40645-019-0261-6
- Dai, B., Jiang, S., Jiang, Y., Zhao, K., Liu, D., 2008. Geochronology, geochemistry and hf-sr-nd isotopic compositions of huziyan mafic xenoliths, southern Hunan Province, south China: petrogenesis and implications for lower crust evolution. Lithos 102 (1), 65–87. https://doi.org/10.1016/j.lithos.2007.08.010.
- Dai, L., Hu, H., Li, H., Jiang, J., Hui, K., 2014. Influence of temperature, pressure, and chemical composition on the electrical conductivity of granite. Am. Mineral. 99 (7), 1420–1428. https://doi.org/10.2138/am.2014.4692.
- Dai, L., Karato, S.-I., 2014. High and highly anisotropic electrical conductivity of the asthenosphere due to hydrogen diffusion in olivine. Earth Planet Sci. Lett. 408, 79–86. https://doi.org/10.1016/j.epsl.2014.10.003.
- Downes, H., Peltonen, P., Manttari, I., Sharkov, E.V., 2002. Properozoic zircon ages from lower crustal granulite xenoliths, kola peninsula, Russia: evidence for crustal growth and reworking. Journal of Geological Society 159 (5), 485–488. https://doi.org/ 10.1144/0016-764901-162.
- Fuji-ta, K., Seki, M., Ichiki, M., 2018. Random network model of electrical conduction in two-phase rock. Mineral. Petrol. 112 (6), 857–864. https://doi.org/10.1007/
- Gatzemeier, A., Tommasi, A., 2006. Flow and electrical anisotropy in the upper mantle: finite-Element models constraints on the effects of olivine crystal preferred orientation and microstructure. Phys. Earth Planet. Inter. 158 (2), 92–106. https://doi.org/10.1016/j.pepi.2006.01.009.
- Gibert, B., Mainprice, D., 2009. Effect of crystal preferred orientations on the thermal diffusivity of quartz polycrystalline aggregates at high temperature. Tectonophysics 465 (1–4), 150–163. https://doi.org/10.1016/j.tecto.2008.11.006.
- Hacker, B.R., Ritzwoller, M.H., Xie, J., 2014. Partially melted, mica-bearing crust in central Tibet. Tectonics 33 (7), 1408–1424. https://doi.org/10.1002/ 2014TC003545.
- Hashin, Z., Shtrikman, S., 1962. A variational approach to the theory of the effective magnetic permeability of multiphase materials. J. Appl. Phys. 33 (10), 3125–3131. https://doi.org/10.1063/1.1728579.
- Heinson, G., White, A., 2005. Electrical resistivity of the northern Australian lithosphere: crustal anisotropy or mantle heterogeneity? Earth Planet Sci. Lett. 232 (1), 157–170. https://doi.org/10.1016/j.epsl.2004.12.029.
- Heise, W., Pous, J., 2003. Anomalous phases exceeding 90° in magnetotellurics: anisotropic model studies and a field example. Geophys. J. Int. 155 (1), 308–318. https://doi.org/10.1046/j.1365-246X.2003.02050.x.
- Hou, C., Liu, J., Zhou, B., Ji, L., Fan, W., Chen, X., Zhang, J., 2023. Fluid-enhanced diffusive mass transfer combined with GBS as an important process for protracted weakening in the middle-lower crust. Journal of Structure Geology 171 (5), 104861. https://doi.org/10.1016/j.jsg.2023.104861.
- Hu, H., Dai, L., Sun, W., Wang, M., Jing, C., 2022. Constraints on fluids in the Continental crust from laboratory-based electrical conductivity measurements of plagioclase. Gondwana Res. 107 (8–9), 1–12. https://doi.org/10.1016/j.gr.2022.02.011.

- Hu, H., Yin, C., Dai, L., Lai, J., Chen, Y., Wang, P., Zhu, J., Han, S., 2024. The role of α-β quartz transition in fluid storage in crust from the evidence of electrical conductivity. J. Geophys. Res. Solid Earth 129 (9), e2024JB029140. https://doi.org/10.1029/2024JB029140.
- Kapinos, G., Montahaei, M., Meqbel, N., Brasse, H., 2016. Three-dimensional electrical resistivity image of the south-central Chilean subduction zone. Tectonophysics 666, 76–89. https://doi.org/10.1016/j.tecto.2015.10.016.
- Kirkby, A., Heinson, G., Krieger, L., 2016. Relating permeablity and electrical resistivity in fractures using random resistor network models. J. Geophys. Res. Solid Earth 121 (3), 1546–1564. https://doi.org/10.1002/2015jb012541.
- Kirkpatrick, S., 1973. Percolation and conduction. Rev. Mod. Phys. 45 (4), 574–588. https://doi.org/10.1103/RevModPhys.45.574.
- Le Pape, F., Jones, A.G., Vozar, J., Wei, W., 2012. Penetration of crustal melt beyond the kunlun fault into northern Tibet. Nat. Geosci. 5 (5), 330–335. https://doi.org/ 10.1038/ngeo1449.
- Leibecker, J., Gatzemeier, A., Hönig, M., Kuras, O., Soyer, W., 2002. Evidence of electrical anisotropic structures in the lower crust and the upper mantle beneath the rhenish shield. Earth Planet Sci. Lett. 202 (2), 289–302. https://doi.org/10.1016/ S0012-821X(02)00783-5
- Liu, S., Xu, Y., Yang, B., Guo, Z., Shi, Y., Liu, Y., 2021. Deciphering fine electrical conductivity structures in the crust from MT data using the equivalent conductivity formula. J. Geophys. Res. Solid Earth 126 (10), e2021JB022519. https://doi.org/ 10.1029/2021JB022519.
- Liu, Y., Junge, A., Yang, B., Löwer, A., Cembrowski, M., Xu, Y., 2019. Electrically anisotropic crust from three-dimensional magnetotelluric modeling in the Western junggar, NW China. J. Geophys. Res. Solid Earth 124 (9), 9474–9494. https://doi. org/10.1029/2019JB017605.
- Mainprice, D., Hielscher, R., Schaeben, H., 2011. Calculating anisotropic physical properties from texture data using the MTEX open-source package. Geological Society, London, Special Publications 360 (1), 175–192. https://doi.org/10.1144/ SP360.10.
- Martí, A., 2013. The role of electrical anisotropy in magnetotelluric responses: from modelling and dimensionality analysis to inversion and interpretation. Surv. Geophys. 35 (1), 179–218. https://doi.org/10.1007/s10712-013-9233-3.
- Montanini, A., Harlov, D., 2006. Petrology and mineralogy of granulite-facies mafic xenoliths (sardinia, Italy): evidence for KCl metasomatism in the lower crust. Lithos 92, 588–608. https://doi.org/10.1016/j.lithos.2006.03.053.
- Passchier, C.W., Trouw, R.A.J., 2005. Microtectonics. Springer Verlag, Berlin, p. 366.
- Pommier, A., Leinenweber, K., Kohlstedt, D.L., Qi, C., Garnero, E.J., Mackwell, S.J., Tyburczy, J.A., 2015. Experimental constraints on the electrical anisotropy of the lithosphere-asthenosphere system. Nature 522 (7555), 202–206. https://doi.org/ 10.1038/nature14502.
- Pommier, A., Le-Trong, E., 2011. "SIGMELTS": a web portal for electrical conductivity calculations in geosciences. Comput. Geosci. 37 (9), 1450–1459. https://doi.org/ 10.1016/j.cageo.2011.01.002.
- Rudnick, R.L., Gao, S., 2003. Composition of the Continental crust. In: Rudnick, R.L. (Ed.), The Crust. Elsevier, Amsterdam, pp. 1–70. https://doi.org/10.1016/B978-0-08-095975-7.00301-6.
- Schulgasser, K., 1976. Relationship between single-crystal and polycrystal electrical conductivity. J. Appl. Phys. 47 (5), 1880–1886. https://doi.org/10.1063/1.322907.
- Shankland, T.J., Duba, A.G., 1990. Standard electrical conductivity of isotropic, homogeneous olivine in the temperature range 1200–1500 °C. Geophys. J. Int. 103 (1), 25–31. https://doi.org/10.1111/j.1365-246X.1990.tb01749.x.
- Simpson, F., 2002. Intensity and direction of lattice-preferred orientation of olivine: are electrical and seismic anisotropies of the Australian mantle reconcilable? Earth Planet Sci. Lett. 203, 535–547. https://doi.org/10.1016/S0012-821X(02)00862-2.
- Simpson, F., 2013. Distribution functions for anisotropic electrical resistivities due to hydrogen diffusivity in aligned peridotite and their application to the lithosphereasthenosphere boundary. Tectonophysics 592, 31–38. https://doi.org/10.1016/j. tecto.2013.02.007.
- Simpson, F., Tommasi, A., 2005. Hydrogen diffusivity and electrical anisotropy of a peridotite mantle. Geophys. J. Int. 160 (3), 1092–1102. https://doi.org/10.1111/ i.1365-246X.2005.02563.x.
- Sodergren, T.L., 2002. Deep Fluid State and Thermal Regime of the Central Great Basin, Nevada, Inferred from Electrical Resistivity. M.S. Thesis. University of Utah, p. 44.
- Sun, W., Dai, L., Li, H., Hu, H., Liu, C., 2019. Effect of temperature, pressure and chemical composition on the electrical conductivity of granulite and geophysical implications. J. Mineral. Petrol. Sci. 114 (2), 87–98. https://doi.org/10.2465/ jmps.181107b.
- Taylor-West, J., Katz, R.F., 2015. Melt-preferred orientation, anisotropic permeability and melt-band formation in a deforming, partially molten aggregate. Geophys. J. Int. 203 (2), 1253–1262. https://doi.org/10.48550/arXiv.1505.00559.
- Ulianov, A., Kalt, A., 2006. Mg-Al sapphirine- and Ca-Al hibonite-bearing granulite xenoliths from the chyulu hills volcanic field, Kenya. J. Petrol. 47 (5), 901–927. https://doi.org/10.1093/petrology/egi100.
- Wang, D., Li, H., Yi, L., Matsuzaki, T., Yoshino, T., 2010. Anisotropy of synthetic quartz electrical conductivity at high pressure and temperature. J. Geophys. Res. 115, B09211. https://doi.org/10.1029/2009JB006695.
- Wang, M., Dai, L., Hu, H., Sun, W., Hu, Z., Jing, C., 2022. Effect of different mineralogical proportions on the electrical conductivity of dry hot-pressed sintering gabbro at high temperatures and pressures. Minerals 12 (3), 336. https://doi.org/10.3390/ min12030336.
- Wannamaker, P.E., 2005. Anisotropy versus heterogeneity in Continental solid Earth electromagnetic studies: fundamental response characteristics and implications for physicochemical state. Surv. Geophys. 26 (6), 733–765. https://doi.org/10.1007/ s10712-005-1832-1.

- Wannamaker, P.E., Doerner, W., Stodt, J., Johnston, J., 1997. Subdued state of tectonism of the great basin interior relative to its eastern margin based on deep resistivity structure. Earth Planet Sci. Lett. 150 (1–2), 41–53. https://doi.org/10.1016/S0012-821X(97)00076-9
- Wannamaker, P.E., Hasterok, D., Johnston, J., Stodt, J., Hall, D., Sodergren, T., Pellerin, L., Maris, V., Doerner, W., Groenewold, K., Unsworth, M., 2008. Lithospheric dismemberment and magmatic processes of the great basin-colorado Plateau transition, Utah, implied from magnetotellurics. G-cubed 9 (5), Q05019. https://doi.org/10.1029/2007GC001886.
- Xu, Y., Shankland, T.J., Poe, B.T., 2000. Laboratory-based electrical conductivity in the Earth's mantle. J. Geophys. Res. 105 (B12), B12. https://doi.org/10.1029/ 2000.IB900299
- Yang, X., 2011. Origin of high electrical conductivity in the lower Continental crust: a review. Surv. Geophys. 32 (6), 875–903. https://doi.org/10.1007/s10712-011-9145-z.
- Yang, X., 2012. Orientation-related electrical conductivity of hydrous olivine, clinopyroxene and plagioclase and implications for the structure of the lower Continental crust and uppermost mantle. Earth Planet Sci. Lett. 317–318, 241–250. https://doi.org/10.1016/j.epsl.2011.11.011.
- Yang, X., Deloule, E., Xia, Q., Fan, Q., Feng, M., 2008. Water contrast between Precambrian and Phanerozoic Continental lower crust in eastern China. J. Geophys. Res. 113 (B8), B08207. https://doi.org/10.1029/2007JB005541.
- Yang, X., Keppler, H., McCammon, C., Ni, H., 2011. Electrical conductivity of orthopyroxene and plagioclase in the lower crust. Contrib. Mineral. Petrol. 163 (1), 33–48. https://doi.org/10.1007/s00410-011-0657-9.
- Zhang, B., Yoshino, T., Yamazaki, D., Manthilake, G., Katsura, T., 2014. Electrical conductivity anisotropy in partially molten peridotite under shear deformation. Earth Planet Sci. Lett. 405, 98–109. https://doi.org/10.1016/j.epsl.2014.08.018.